

Elasto-plastic analysis of discontinuous medium using linearly conforming radial point interpolation method

S.M. Binesh^{a*}, N. Hataf^b, A. Ghahramani^b

^aCivil and Environmental Engineering Dept., Shiraz University of Technology

^bCivil and Environmental Engineering Dept., Shiraz University

Received 4 February 2013; accepted in revised form 11 May 2013

Abstract

In this paper, the linearly conforming enriched radial basis point interpolation method is implemented for the elasto-plastic analysis of discontinuous medium. The linear conformability of the method is satisfied by the application of stabilized nodal integration and the enrichment of radial basis functions is achieved by the addition of linear polynomial terms. To implement the method for the analysis of a discontinuous medium, an interface layer is assumed between different materials. Interfaces are simulated by the concept of linkage element and there is no need of node or element in the traditional sense. The stiffness of each interface layer has been taken into account by defining normal and tangential stiffness coefficients along the layer. The displacement of each point across the interface layer is tied to the displacement of surrounding material nodes. The final system of equations is derived by the combination of equations for different parts of a discontinuous medium in the global coordinate. Based on the derived equations a computer code has been developed and the results of analysis with the mesh-free method are compared with the results of the finite element analysis and experimental tests.

Keywords: meshfree method, radial point interpolation, nodal integration, discontinuous medium.

1. Introduction

Recently a great deal of research has been devoted to the application of meshfree methods in different fields of science [1-3]. The main objective of meshfree methods is to get rid of the deficiencies related to mesh definition. All these meshfree methods can be classified collectively as Galerkin meshfree method [4-9], Petrov-Galerkin meshfree method [10], or collocation meshfree method [11]. Among these, a majority of meshfree methods are based on Galerkin procedure, such as element free Galerkin [4], reproducing kernel particle method [5], point interpolation method [6] and so on [7-9].

Gaussian integration is commonly used in Galerkin meshfree methods for integration of the weak form. However due to the complexity involved in the Gauss integration, attempts have been made to develop nodal integration for meshfree computation. Nodal integration encounters spatial instability due to under integration and vanishing derivatives of meshfree shape functions at nodes. Several methods have been introduced as a correction or stabilization of nodal integration. Beissel and Belytschko [12] proposed a stabilization

*Corresponding author.

E-mail address: smbinesh@yahoo.com

technique by adding the square of the residual of the equilibrium equation to the potential energy. Although the addition of stabilization term improves the accuracy of solution for the problems with spurious near-singular modes, for problems that do not contain unstable modes in their original solution, this addition actually deteriorate the accuracy. Randles et al. [13] introduced stress point method to improve the accuracy and to reduce spurious oscillations in SPH. Bonet and Kulasegaram [14] presented a correction term into the derivatives of shape function at nodal points to eliminate the spurious modes in SPH. Chen et al. [15] pointed out that the inaccuracy in solution by the nodal integration is due to the disobedience of the integral identity given by the divergence theorem. They proposed a conforming strain smoothing in a stabilized conforming nodal integration (SCNI) in which the strain at a specific point is replaced with the average strain in a Voronoi cell that contains the point. Divergence theorem is then used to replace the area, or volume integration around the point by a contour integration of the Voronoi cell boundary.

The objective of this work is to combine the SCNI and the radial point interpolation method (RPIM) to analyze a discontinuous medium in elasto-plastic behavior of materials. The outline of this paper is as follows: the mesh-free method used in this paper, i.e. RPIM is reviewed in section 2, general equations for modeling a discontinuous medium is proposed in section 3, stabilized conforming nodal integration is presented in section 4, section 5 demonstrates the effectiveness of proposed methodology by solving examples and, conclusions are discussed in section 6.

2. Radial basis point interpolation method

A field function $u(\mathbf{x})$ can be approximated using both radial and polynomial basis as

$$u(\mathbf{x}) = \sum_i^n R_i(\mathbf{x})a_i + \sum_j^m P_j(\mathbf{x})b_j = \mathbf{R}^T(\mathbf{x})\mathbf{a} + \mathbf{P}^T(\mathbf{x})\mathbf{b} \quad (1)$$

where, n is the number of field nodes in the local support domain for point \mathbf{x} and the vector $\mathbf{R}(\mathbf{x})$ is defined as:

$$\mathbf{R}(\mathbf{x}) = [R_1(\mathbf{x}), \dots, R_k(\mathbf{x}), \dots, R_n(\mathbf{x})]^T \quad (2)$$

where,

$$R_k(\mathbf{x}) = R(r_k) \quad (3)$$

is the radial basis functions and

$$r_k = \left[(x_k - x)^2 + (y_k - y)^2 \right]^{\frac{1}{2}} \quad (4)$$

is the distance between the point \mathbf{x} and field node \mathbf{x}_k and vector

$$\mathbf{P}(\mathbf{x}) = [P_1(\mathbf{x}), P_2(\mathbf{x}), \dots, P_m(\mathbf{x})]^T \quad (5)$$

is the vector of polynomial basis functions in 2D space $\mathbf{x}^T = [x, y]$, and m is the number of terms of polynomial basis functions. Vectors \mathbf{a} and \mathbf{b} , where,

$$\mathbf{a} = [a_1, a_2, \dots, a_n]^T \quad (6)$$

$$\mathbf{b} = [b_1, b_2, \dots, b_m]^T \quad (7)$$

are, respectively, coefficients for $\mathbf{R}(\mathbf{x})$ and $\mathbf{P}(\mathbf{x})$. The radial basis functions are used to guarantee the invertability of moment matrix, and the polynomial basis functions are used to ensure the linear consistency of generated shape functions. The coefficient vectors \mathbf{a} and \mathbf{b} are determined by enforcing equation (1) to be satisfied at all the n nodes within the local support domain. By the lengthy but straightforward procedure given by Liu [16] we have

$$\mathbf{u}(\mathbf{x}) = \mathbf{\Phi}(\mathbf{x})\mathbf{U}_s \quad (8)$$

where,

$$\mathbf{U}_s = [u_1, u_2, \dots, u_n]^T \quad (9)$$

is a vector of nodal values of the field variable in the local support domain, and

$$\mathbf{\Phi}(\mathbf{x}) = [\varphi_1(\mathbf{x}), \varphi_2(\mathbf{x}), \dots, \varphi_n(\mathbf{x})] \quad (10)$$

contains RPIM shape functions for the n local nodes in which $\varphi_k(\mathbf{x})$ is as follows:

$$\varphi_k(\mathbf{x}) = \sum_i^n R_i(\mathbf{x})S_{aik} + \sum_j^m P_j(\mathbf{x})S_{bjk} \quad (11)$$

where, S_{aik} is the (i, k) entry of matrix \mathbf{S}_a where,

$$\mathbf{S}_a = \mathbf{R}_M^{-1} - \mathbf{R}_M^{-1} \mathbf{P}_M \mathbf{S}_b \quad (12)$$

and S_{bjk} is the (j, k) entry of matrix \mathbf{S}_b where,

$$\mathbf{S}_b = (\mathbf{P}_M^T \mathbf{R}_M^{-1} \mathbf{P}_M)^{-1} \mathbf{P}_M^T \mathbf{R}_M^{-1} \quad (13)$$

The moment matrices \mathbf{R}_M and \mathbf{P}_M consisted of row vectors $\mathbf{R}^T(x_i)$ and $\mathbf{P}^T(x_i)$ ($i=1,2,\dots,n$) respectively.

There are many types of radial basis functions. In this paper the multi-quadratic form is used as:

$$R(r_i) = (r_i^2 + c^2)^q \quad (14)$$

where, c and q are shape parameters which are, respectively, proposed 1.42 and 0.98 by Liu [16] for solid mechanics problems..

3. General equations for the elasto-plastic modeling of discontinuous medium

(a) System of equations

The total potential energy functional for a discontinuous medium can be expressed as

$$\Pi = \Pi_m + \Pi_i + \Pi_F \quad (15)$$

where, Π_m and Π_i are respectively, the elastic strain energy of each continuous media and the interface layers between different materials, and Π_F is the potential energy related to the external forces. These functionals are

$$\Pi_m = \iint_{\Omega_m} \frac{1}{2} \boldsymbol{\varepsilon}_m^T \boldsymbol{\sigma}_m d\Omega_m \quad (16)$$

$$\Pi_i = \iint_{\Omega_i} \frac{1}{2} \boldsymbol{\varepsilon}_i^T \boldsymbol{\sigma}_i d\Omega_i \quad (17)$$

$$\Pi_F = - \int_{\Gamma_m} \mathbf{U}^T \bar{\mathbf{T}} d\Gamma_m - \iint_{\Omega_m} \mathbf{U}^T \mathbf{b} d\Omega_m \quad (18)$$

where, $\boldsymbol{\varepsilon}_m$ and $\boldsymbol{\sigma}_m$ are respectively, the strain and stress tensors related to the continua

$$\boldsymbol{\varepsilon}_m^T = \{ \varepsilon_x \ \varepsilon_y \ \gamma_{xy} \} \quad , \quad \boldsymbol{\sigma}_m^T = \{ \sigma_x \ \sigma_y \ \tau_{xy} \} \quad (19)$$

The $\boldsymbol{\varepsilon}_i$ and $\boldsymbol{\sigma}_i$ are respectively, the strain and stress tensors across the interface layers, \mathbf{U} is the displacement vector, $\bar{\mathbf{T}}$ is the prescribed boundary traction and \mathbf{b} is the body force vector. Ω_m and Ω_i stand for the continuous material and interface layer domains respectively. Γ_m is

the material boundary on which the external tractions are imposed. It should be noted that subscript m and i stand for the material and interface media respectively.

Considering the Hook's law (i.e. $\boldsymbol{\sigma} = \mathbf{D}\boldsymbol{\varepsilon}$), the variational form of equation (15) can be written as

$$\delta\Pi = \iint_{\Omega_m} (\delta\boldsymbol{\varepsilon}_m)^T \mathbf{D}_m \boldsymbol{\varepsilon}_m d\Omega_m + \iint_{\Omega_i} (\delta\boldsymbol{\varepsilon}_i)^T \mathbf{D}_i \boldsymbol{\varepsilon}_i d\Omega_i - \iint_{\Omega_m} (\delta\mathbf{U})^T \mathbf{b} d\Omega_m - \int_{\Gamma_m} (\delta\mathbf{U})^T \bar{\mathbf{T}} d\Gamma_m = 0 \quad (20)$$

where, \mathbf{D}_m and \mathbf{D}_i are the elasticity matrices for materials and interface layers respectively. The elasticity matrix for continuous mediums in plane strain condition can be written as

$$\mathbf{D}_B = \frac{E(1-\nu)}{(1+\nu)(1-2\nu)} \begin{bmatrix} 1 & \frac{\nu}{1-\nu} & 0 \\ \frac{\nu}{1-\nu} & 1 & 0 \\ 0 & 0 & \frac{1-2\nu}{2(1-\nu)} \end{bmatrix} \quad (21)$$

where, E and ν are elasticity modulus and Poisson's ratio respectively. The constitutive matrix for interface layer will be derived later in this section.

The discrete form of equations can be obtained by the imposition of the strain-displacement relation and equation (8) into equation (20). For the continuous material the strain-displacement relation can be easily written as

$$\boldsymbol{\varepsilon} = \mathbf{B}\mathbf{U}_s \quad (22)$$

where,

$$\mathbf{B} = \begin{bmatrix} \mathbf{B}_{i1} & \mathbf{B}_{i2} & \dots & \mathbf{B}_{i3} & \dots & \mathbf{B}_{in} \end{bmatrix} \quad (23)$$

and

$$\mathbf{B}_{ik} = \begin{bmatrix} \frac{\partial\phi_{ik}}{\partial x} & 0 & \frac{\partial\phi_{ik}}{\partial y} \\ 0 & \frac{\partial\phi_{ik}}{\partial y} & \frac{\partial\phi_{ik}}{\partial x} \end{bmatrix}^T \quad (24)$$

where, $\phi_{ik} = \phi_k(x_i)$ is the shape function of kth node at ith node in the support domain. However the derivation of stress-strain relation and also the strain-displacement relation in the interface layer requires some manipulations.

As shown in Figure 1 the interface layer can be considered as a layer with two stiffness coefficients along two orthogonal directions (i.e. K_s and K_n). According to Figure 1, the relative deformation vector $\boldsymbol{\delta}$ at point P between the top and bottom surfaces can be related to the displacements of points A and B. Hence it can be written as

$$\boldsymbol{\delta} = \begin{bmatrix} \delta_s \\ \delta_n \end{bmatrix} = \bar{\mathbf{U}}_A - \bar{\mathbf{U}}_B = \begin{bmatrix} u_A - u_B \\ v_A - v_B \end{bmatrix} \quad (25)$$

where, δ_s and δ_n are respectively, the shear and normal relative displacement at point P. $\bar{\mathbf{U}}_A$ and $\bar{\mathbf{U}}_B$ are the displacement vectors in the local coordinate n-s at points A and B respectively.

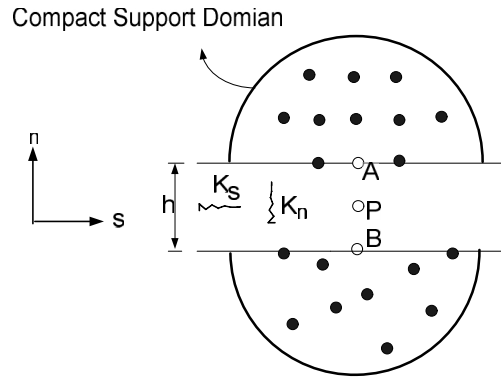


Figure 1. Interface layer modeling by linkage element concept

Considering the relation between local and global coordinate, we have

$$\bar{\mathbf{U}} = \mathbf{L}\mathbf{U} \quad (26)$$

where, \mathbf{L} is coordinate transform matrix, \mathbf{U} is the displacement vector in the global coordinate.

As shown in Figure 1 the field variable (i.e. displacement) at points A and B can be estimated by the values at the nodes located in the compact support domains. According to equations (8), (25) and (26) we have

$$\boldsymbol{\delta} = \mathbf{B}_i \mathbf{U}_s \quad (27)$$

where, \mathbf{U}_s is the displacement vector composed of displacement at all nodes in the compact support domains of point A and B

$$\mathbf{B}_i = [-\mathbf{L}\boldsymbol{\Phi}_A \quad \mathbf{L}\boldsymbol{\Phi}_B] \quad (28)$$

where, $\boldsymbol{\Phi}_A$ and $\boldsymbol{\Phi}_B$ are the shape function matrices of the nodes in the support domains of point A and B respectively

Neglecting the normal strain component in the s direction, the strain vector in the local coordinate can be defined as

$$\boldsymbol{\varepsilon} = \frac{1}{h} \boldsymbol{\delta} \quad (29)$$

where, h is the virtual thickness assumed for the interface layer and $\boldsymbol{\varepsilon} = [\gamma_{ns} \quad \varepsilon_n]^T$, in which ε_n is the normal strain in the direction n , and γ_{ns} is the shear strain. By substituting equation (29) into equation (27) the relation between strain and nodal displacement can be obtained as

$$\boldsymbol{\varepsilon} = \mathbf{B}_I \mathbf{U}_s \quad (30)$$

where,

$$\mathbf{B}_I = \left(\frac{1}{h} \right) \mathbf{B}_i \quad (31)$$

To evaluate the stiffness matrix related to the interface layer, the relation between stress and strain in this region is also needed. According to Figure 1 the relation between stress vector and relative deformation can be written as

$$\boldsymbol{\sigma} = \mathbf{D}_i \boldsymbol{\delta} \quad (32)$$

where, the stress vector $\boldsymbol{\sigma}$ consists of the normal stress σ_n and the tangential stress τ in the interface region.

$$\boldsymbol{\sigma} = [\boldsymbol{\tau} \quad \sigma_n]^T \tag{33}$$

Matrix \mathbf{D}_f can also be defined as

$$\mathbf{D}_i = \begin{bmatrix} K_s & 0 \\ 0 & K_n \end{bmatrix} \tag{34}$$

Substituting equation (29) into equation (32) gives

$$\boldsymbol{\sigma} = \mathbf{D}_I \boldsymbol{\varepsilon} \tag{35}$$

where,

$$\mathbf{D}_I = h\mathbf{D}_i \tag{36}$$

At this stage all relations between stress, strain and displacement at the continuous domains and interface layers are known and equation (20) can be rewritten as

$$[\iint_{\Omega_m} \mathbf{B}_m^T \mathbf{D}_m \mathbf{B}_m d\Omega_m + \iint_{\Omega_i} \mathbf{B}_I^T \mathbf{D}_I \mathbf{B}_I d\Omega_i] \mathbf{U}_S = \iint_{\Omega_m} \boldsymbol{\Phi}^T \mathbf{b} d\Omega_m + \int_{\Gamma_m} \boldsymbol{\Phi}^T \bar{\mathbf{T}} d\Gamma_m \tag{37}$$

Assuming constant virtual thickness for the interface layers, equation (37) can be written as

$$[\mathbf{K}_m + \mathbf{K}_i] \mathbf{U}_S = \mathbf{F}$$

(38)

where,

$$\mathbf{K}_m = \iint_{\Omega_m} \mathbf{B}_m^T \mathbf{D}_m \mathbf{B}_m d\Omega_m \tag{39}$$

$$\mathbf{K}_i = \int_{\beta} \mathbf{B}_I^T \mathbf{D}_I \mathbf{B}_I d\beta$$

(40)

$$\mathbf{F} = \iint_{\Omega_m} \boldsymbol{\Phi}^T \mathbf{b} d\Omega_m + \int_{\Gamma_m} \boldsymbol{\Phi}^T \bar{\mathbf{T}} d\Gamma_m \tag{41}$$

where, β is the length parameter along the interface layer.

(b) Elastic-plastic relation

The elastic-perfectly plastic Mohr-Coulomb criterion has been used in this paper and the yield function is as follows:

$$F = (\sigma_1 - \sigma_3) - 2\zeta \cos(\Theta) + (\sigma_1 + \sigma_3) \sin(\Theta) \tag{42}$$

where, σ_1 and σ_3 are the principle stresses, ζ is the cohesion and Θ is the internal friction angle. Substituting Ψ (dilation angle) for Θ , the potential function would be obtained. Considering the yield (\mathbf{F}) and potential (\mathbf{G}) functions, the relation between the stress and strain increment can be written as:

$$d\boldsymbol{\sigma} = (\mathbf{D}^e + R(\mathbf{D}^{ep} - \mathbf{D}^e)) d\boldsymbol{\varepsilon} \tag{43}$$

where, \mathbf{D}^e is the elasticity matrix and

$$\mathbf{D}^{ep} = \left[\begin{array}{c} \mathbf{D}^e \left\{ \frac{\partial \mathbf{G}}{\partial \boldsymbol{\sigma}} \right\} \left\{ \frac{\partial \mathbf{F}}{\partial \boldsymbol{\sigma}} \right\}^T \mathbf{D}^e \\ \left\{ \frac{\partial \mathbf{F}}{\partial \boldsymbol{\sigma}} \right\}^T \mathbf{D}^e \left\{ \frac{\partial \mathbf{G}}{\partial \boldsymbol{\sigma}} \right\} \end{array} \right] \tag{44}$$

Parameter R is defined as:

$$R = \frac{F_{New}}{F_{New} - F_{Old}} \quad (45)$$

where, F_{New} and F_{Old} are, respectively, the values of yield function for the new and the old state of stresses. When the two successive states of stresses are in elastic region, $R = 0$, and when the both successive states of stresses are in plastic region, $R = 1$.

4. Stabilized conforming nodal integration

For the linear exactness in Galerkin approximation, the method of shape function construction and, the method of integration of the weak form have to be linear consistent. The former condition is satisfied by the augmentation of linear polynomial terms with the radial basis of point interpolation method. For linear consistency of the integration method, integration constrains must be satisfied. According to the research of Chen et al. [15], by satisfying the linear exactness for a standard patch test, the integration constrains would be obtained as follows:

$$\iint_{\Omega} \mathbf{B}_I^T d\Omega = \int_{\Gamma} \mathbf{N}_I^T d\Gamma \quad (46)$$

where, \mathbf{B}_I is the gradient matrix, Ω is the domain of problem, and Γ is the boundary of problem. Matrix \mathbf{N}_I is

$$\mathbf{N}_I = \begin{bmatrix} \phi_1 n_1 & 0 \\ 0 & \phi_2 n_2 \\ \phi_1 n_2 & \phi_2 n_1 \end{bmatrix} \quad (47)$$

where, n_1 and n_2 are the components of outward normal vector to the boundary surface along 1 and 2 axes respectively.

According to Chen's approach, the gradient of field function (displacement) at a node is smoothed by integration over the local domain such as the Voronoi cell, which satisfies the integration constrains and subsequently guarantees the exact linear displacement solution. So they called the method, "*strain smoothing method*" and introduced it as follows:

The smoothed strain can be produced by

$$\tilde{\varepsilon}_{ij}^h(\mathbf{x}_L) = \int_{\Omega} \varepsilon_{ij}^h \Psi(\mathbf{x}; \mathbf{x} - \mathbf{x}_L) d\Omega \quad (48)$$

where, ε_{ij}^h is the strain obtained from displacement by compatibility

$$\varepsilon_{ij}^h = \frac{1}{2} \left(\frac{\partial u_i}{\partial x_j} + \frac{\partial u_j}{\partial x_i} \right) \quad (49)$$

and Ψ is a distribution function which is chosen as

$$\Psi(\mathbf{x}; \mathbf{x} - \mathbf{x}_L) = \begin{cases} \frac{1}{A_L} & \mathbf{x} \in \Omega_L \\ 0 & \mathbf{x} \notin \Omega_L \end{cases} \quad (50)$$

where, A_L is the area of the representative domain of node L obtained from the Voronoi diagram. Combination of equations (8) and (48) to (50) and applying the integration by parts gives:

$$\tilde{\varepsilon}^h(\mathbf{x}_L) = \sum_{I \in G_L} \mathbf{B}_I(\mathbf{x}_L) \mathbf{U}_I \quad (51)$$

where, G_L is a group of nodes in which their associated shape function supports, cover node L. In two dimensional space we have

$$\tilde{\boldsymbol{\varepsilon}}^h = \left[\tilde{\varepsilon}_x^h, \tilde{\varepsilon}_y^h, 2\tilde{\varepsilon}_{xy}^h \right]^T \tag{52}$$

$$\mathbf{U}_I = \left[U_{xI}, U_{yI} \right]^T \tag{53}$$

$$\mathbf{B}_I(\mathbf{x}_L) = \begin{bmatrix} \tilde{b}_{Ix}(\mathbf{x}_L) & 0 \\ 0 & \tilde{b}_{Iy}(\mathbf{x}_L) \\ \tilde{b}_{Iy}(\mathbf{x}_L) & \tilde{b}_{Ix}(\mathbf{x}_L) \end{bmatrix} \tag{54}$$

$$\tilde{b}_{Ix}(\mathbf{x}_L) = \frac{1}{A_L} \int_{\Gamma_L} \varphi_I(\mathbf{x}) n_x(\mathbf{x}) d\Gamma \tag{55}$$

$$\tilde{b}_{Iy}(\mathbf{x}_L) = \frac{1}{A_L} \int_{\Gamma_L} \varphi_I(\mathbf{x}) n_y(\mathbf{x}) d\Gamma \tag{56}$$

As shown in Figure 2, Γ_L is the boundary of Voronoi cell which contains node L. n_x and n_y are, respectively, the x and y components of vector \mathbf{n} (outward vector which is normal to boundary of Voronoi cell). Note that in equation (54) no derivatives of shape functions are involved in evaluating the smoothed gradient matrix at the nodal points. Considering the equation (54) and the nodal integration method, the coefficient matrices of equation (38) can be rewritten as:

$$\mathbf{K}_{IJ} = \sum_{L=1}^{NP} \mathbf{B}_I^T(\mathbf{x}_L) \mathbf{D} \mathbf{B}_J(\mathbf{x}_L) A_L + \mathbf{K}^i \tag{57}$$

$$\mathbf{F}_I = \sum_{L=1}^{NP} \varphi_I(\mathbf{x}_L) \mathbf{b} A_L + \sum_{L=1}^{NPb} \varphi_I(\mathbf{x}_L) \bar{\mathbf{T}} S_L \tag{58}$$

where, NP is the number of points in the local support domain of Node L, NPb is the number of points on the natural boundary, S_L are the weights associated with the boundary points that can also be obtained from the Voronoi diagram, and \mathbf{K}^i is the stiffness matrix of the interface layer .

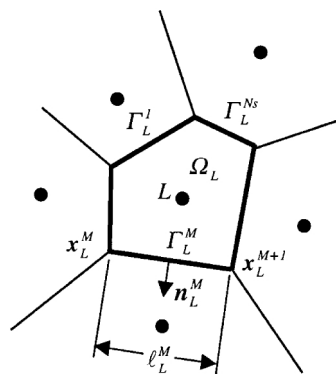


Figure 2. The Voronoi cell contains node L [12]

To calculate equations (55) and (56), any numerical integration method can be used. For instance, by applying a two-point trapezoidal rule for each segment in Figure 2, equations (55) and (56) can be written as

$$\tilde{b}_{ix}(\mathbf{x}_L) = \frac{1}{A_L} \sum_{M=1}^{N_s} \left[\varphi_1(\mathbf{x}_L^M) n_{xL}^M \frac{l_L^M}{2} + \varphi_1(\mathbf{x}_L^{M+1}) n_{xL}^M \frac{l_L^M}{2} \right] \quad (59)$$

$$\tilde{b}_{iy}(\mathbf{x}_L) = \frac{1}{A_L} \sum_{M=1}^{N_s} \left[\varphi_1(\mathbf{x}_L^M) n_{yL}^M \frac{l_L^M}{2} + \varphi_1(\mathbf{x}_L^{M+1}) n_{yL}^M \frac{l_L^M}{2} \right] \quad (60)$$

where, N_s is the total number of segments of Voronoi cell contains node L , \mathbf{x}_L^M and \mathbf{x}_L^{M+1} are the two end points of boundary segment Γ_L^M and l_L^M is the length of Γ_L^M . n_{xL}^M and n_{yL}^M are, respectively, the x and y components of the outward surface normal of Γ_L^M .

5. Numerical study

In this section three example are investigated. In the first example an elastic discontinuous media is assumed and the accuracy and convergence of proposed mesh-free method is investigated. The two latter examples are devoted to the elasto-plastic behaviour of materials and the accuracy of obtained results.

Example 1. Elastic discontinuous media

An elastic discontinuous media shown in Figure 3 is analyzed under depicted loading condition. The elastic properties of material types are shown in Table 1. Between different materials, interface layers are assumed, and the normal and shear stiffness of these layers are 104 kN/m^3 and 106 kN/m^3 respectively.

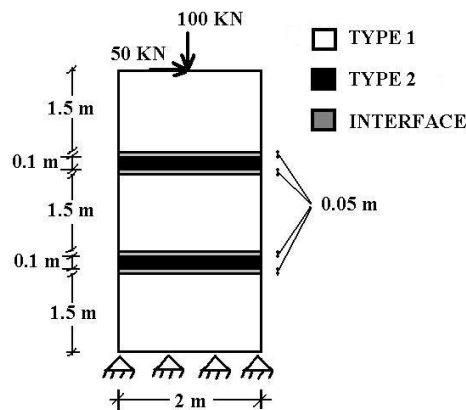


Figure 3. Elastic discontinuous media

Table 1. Material properties

Type number	Elastic modulus (GPa)	Poisson's ratio
TYPE 1	3	0.3
TYPE 2	60	0.25

The results of finite element analysis are used as a datum for comparison. However it is assumed that by increasing the number of elements the results of the finite element code get closer to the exact solution. Hence, parameter η is defined as:

$$\eta = \frac{\left\| \mathbf{U}_{FEM}^P - \mathbf{U}_{FEM}^F \right\|}{\left\| \mathbf{U}_{FEM}^F \right\|} \quad (61)$$

where, $\|\cdot\|$ stands for Euclidean norm, \mathbf{U}_{FEM}^P and \mathbf{U}_{FEM}^F are the vectors of displacement for the analysis with P number of elements and the analysis with the initial number of elements respectively. As in the two successive modeling with increasing number of elements, the value of η remains constant, the results of the analysis can be assumed to be the best for the finite element analysis. Figure 4 shows the variation of η with respect to the number of elements. According to this Figure, the finite element model with 3420 elements gives the best results.

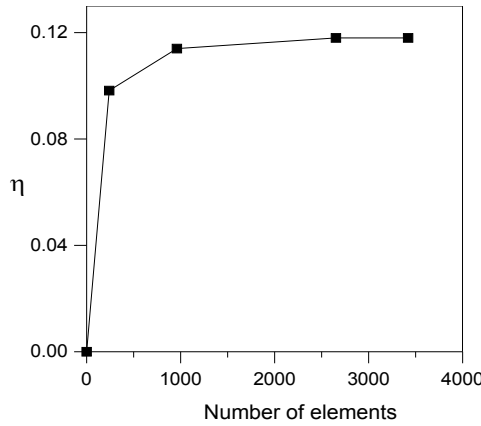


Figure 4. Variation of η with respect to the number of elements

To investigate the convergence of proposed method, three mesh-free models and their Voronoi diagrams are assumed (Figure 5). The first model contains 39 nodes which are 1 m apart from each other. In the second and third models the distances between nodes decreased to 0.5 m and 0.25 m respectively, and consequently 95 and 225 nodes are generated. The relative error of displacement between the mesh-free and the FEM is determined by

$$e_d = \sqrt{\frac{\sum (\mathbf{U}^{FEM} - \mathbf{U}^{MFM})^2}{\sum (\mathbf{U}^{FEM})^2}} \quad (62)$$

where, e_d is the relative error of displacement, \mathbf{U}^{MFM} is the displacement vector in mesh-free method, \mathbf{U}^{FEM} is the displacement vector in FEM. Figure 6 shows the variation of e_d with respect to the distances between nodes. It is obvious that by decreasing the distances between nodes, the relative error is also decreased. This condition confirms the convergence of the method.

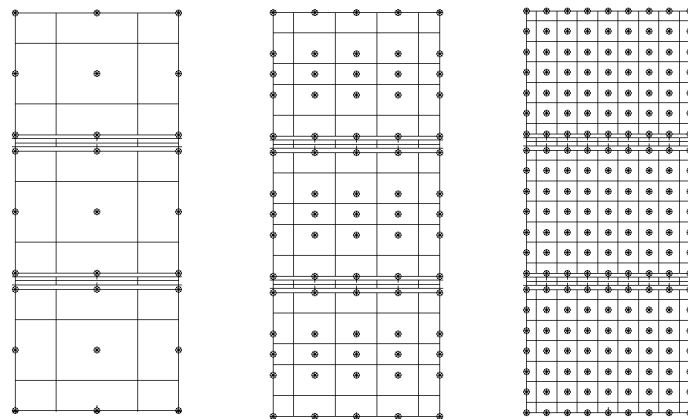


Figure 5. Mesh-free models

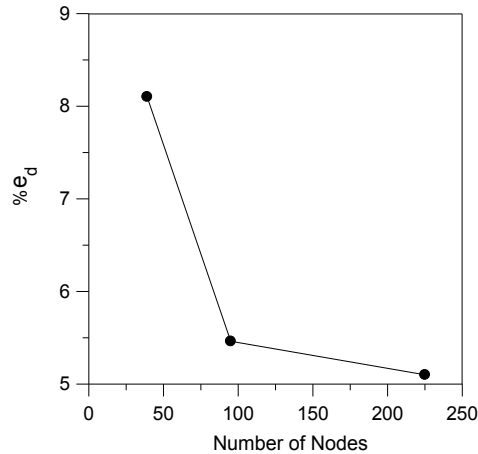


Figure 6. Variation of e_d with respect to the number of nodes

In the last part of this example the stability of the proposed method to the nodes arrangement is investigated. An irregular arrangement of nodes is considered for 225 nodes model and the Voronoi diagram of the model is established as shown in Figure 7. The parameter e_d is calculated for different radiuses of support and the results are represented in Figure 8 for regular and irregular nodal arrangements. As it is obvious from this Figure, the disturbance in nodal arrangement deteriorates the accuracy of results, but the decrease in accuracy is not to that extent to destroy the stability of the proposed method.

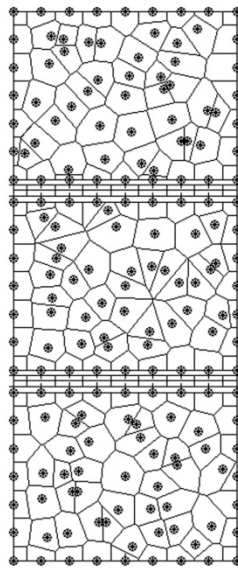


Figure 7. Irregular nodal arrangement

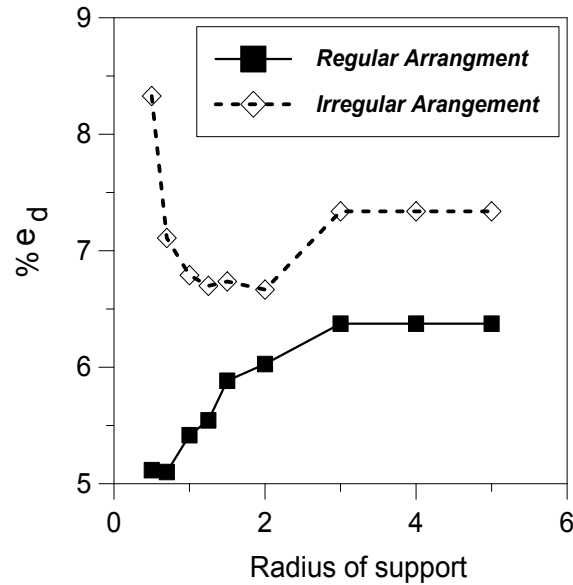


Figure 8. Effect of nodal arrangement on the value of e_d

Example (2) : Thin layers of elastic material surrounded by elasto-plastic media

In this example three thin layers of elastic material are assumed to be surrounded by a cohesive-frictional material. The geometry and loading condition of problem are shown in Figure 9. The cohesive-frictional material is assumed weightless with the elasto-perfectly plastic Mohr-Coulomb parameters of:

elastic modulus=30 MPa , Poisson ratio= 0.3, cohesion= 20 kPa , friction angle= 25°.

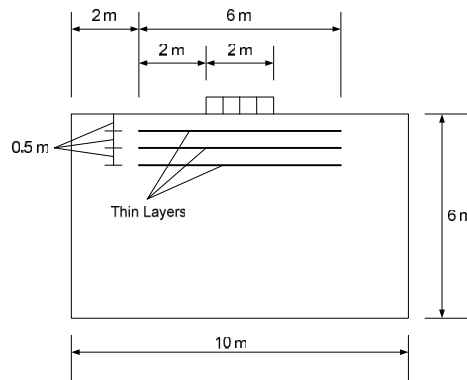
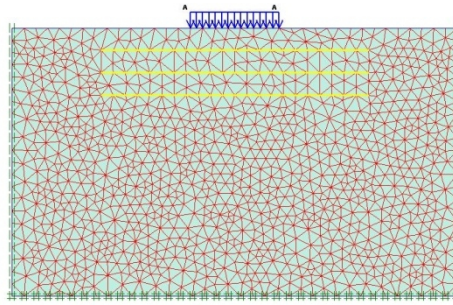


Figure 9. thin layers of elastic material surrounded by elasto-plastic medium

The elastic modulus and a Poisson's ratio of thin layers are 600 MPa and 0.3 respectively. The thickness of layers is considered 0.01m. Complete bound between different domains is assumed.

To investigate the accuracy of proposed mesh-free method, the results of analyses are compared with the results of finite element modeling. The finite element modeling is carried out using the PLAXIS [17] software which can model the thin layers efficiently. The finite element model contains 2182 elements (Figure 10) and it is used as a datum for comparison.



(c)

Figure 10. Finite element model

In meshfree modeling, 360 nodes with regular arrangement are used (Figure 11). Each layer is simulated by 26 nodes along two parallel lines (which are separated from each other by the thickness of layer). The Voronoi diagram for integration is presented in Figure 11. To guarantee that sufficient and suitable nodes are covered in the support domains, the radiuses of the support domains is specially devised with a slightly adjustable value in the program which is automatically self-tuned such that at least 15 nodes are selected for each local support domain.

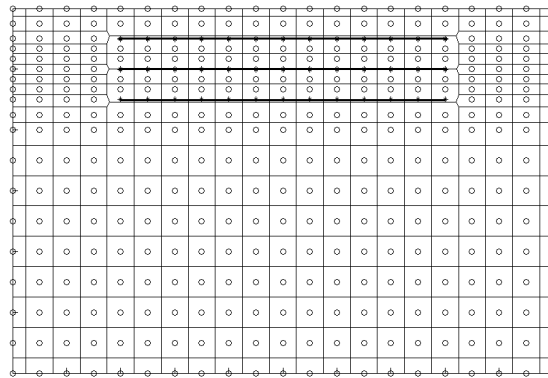


Figure 11. Mesh-free model and Voronoi diagram

The load-deformation curves at the center line beneath the loaded area obtained from both models and represented in Figure 12. The mean root square error (MRSE) between these curves is also computed and shown in the Figure. As it is obvious, there is a very good agreement between the results of finite element with a high number of elements (2182 elements), and meshfree modeling with quite a low number of nodes (360 nodes). The value MRSE implies that the average difference between the values along two curves is just about 3% which is a small error.

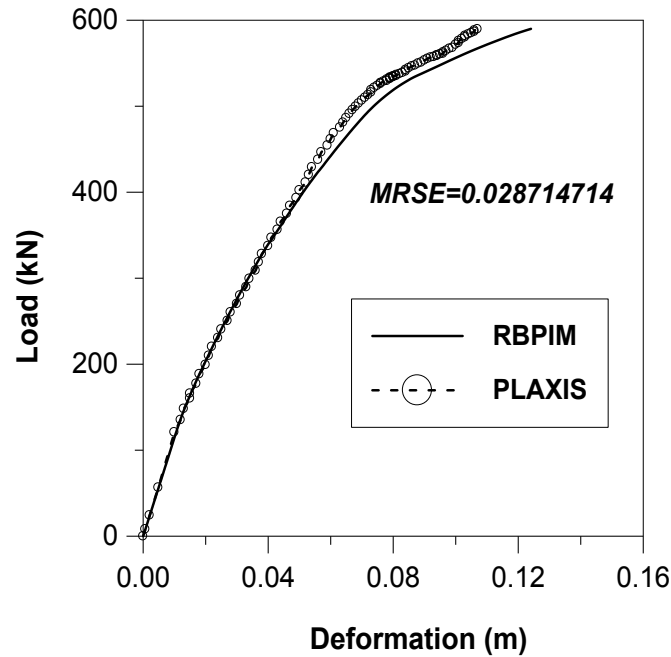


Figure 12. Load-deformation curves for meshfree and finite element models

Example (3) : Pull-out test

One of the most popular tests for the studying of interface behaviour between different materials is pull-out test. In this test a single bar or fiber is pulled out off the surrounding matrix and the corresponding load versus displacement relation is recorded. In order to compare the results of proposed meshfree method with the experimental results, the study of Yogarajah and Yeo [18] is considered. In this research the load and strain distribution is measured along the reinforcement, during a pull-out operation. The schematic layout of test apparatus is shown in Figure 13. The steel tank is filled by sand with the density of 17.5 kN/m^3 , the friction angle of 47° , the elasticity modulus of 80 MPa and null cohesion. A 1.1 m geo-grid with the elasticity modulus of 40 MPa is placed at the mid-height of the tank. The test is performed under displacement-control condition and hence, the load and strain distribution is obtained for 10 mm and 20 mm edge displacement of the reinforcement. The tests are carried out with a uniform overburden pressure of 6.5 kPa and at a displacement rate of 1 mm/min . Detailed description of the test can be seen in [18].

There is also a numerical simulation of the operation by the finite element method. The model of finite element analysis is shown in Figure 14.

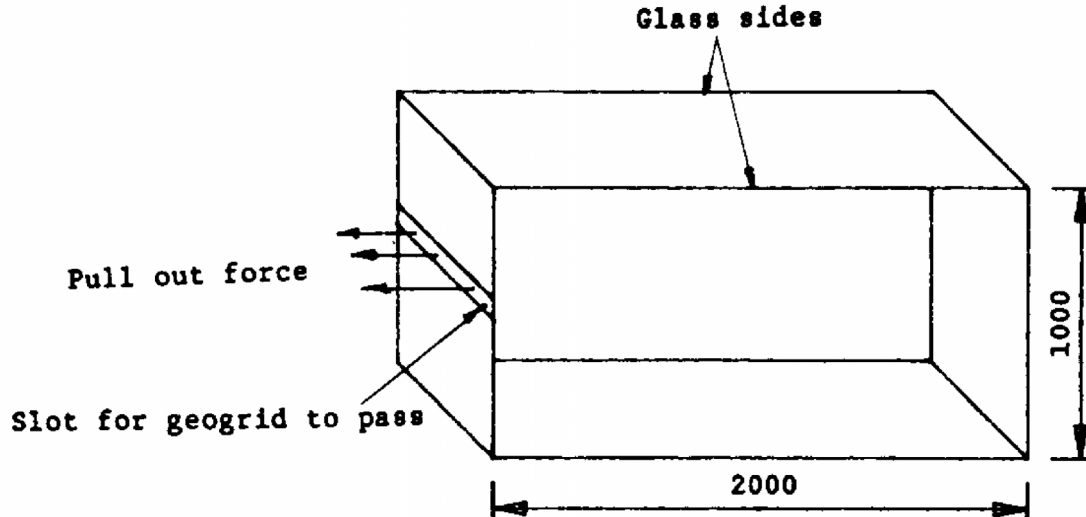


Figure 13. Schematic layout of test apparatus [16]

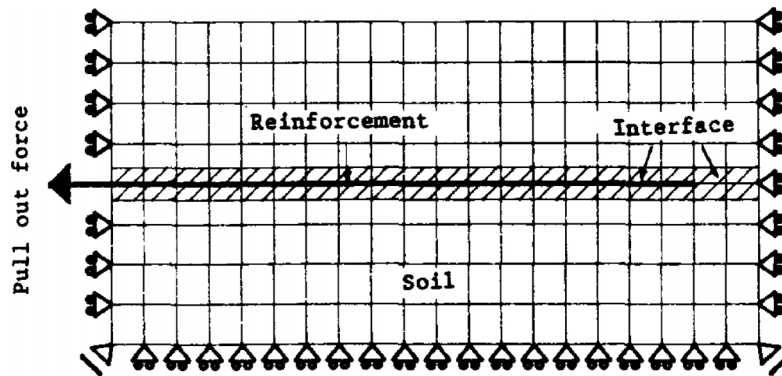


Figure 14. Finite element model of pull-out test [15]

The meshfree model of pull-out test is constructed by 252 nodes for soil and 24 nodes for reinforcement. The soil is assumed to behave under elasto-perfectly plastic Mohr-Coulomb criterion. The nodes arrangement and Voronoi diagram of mesh-free method is presented in Figure 15.

For the meshfree analyses the radius of the support domain is adjusted for two cases. In the first one the value of the radius is automatically self-tuned such that at least 4 nodes are selected for each local support domain. For the second case the supports in the soil media and reinforcement contain at least 15 and 7 nodes respectively. The results of analyses are shown in Figures 16 and 17. In these Figures the results of numerical and experimental investigation of Yogorajah and Yeo is also presented. As it is obvious the results of numerical analyses for the load distributions have a good agreement with the experimental results. Among numerical analyses, the meshfree analysis with at least 15 nodes in each support gives better compatibility with experimental results for 10mm edge displacement of reinforcement. However in 20mm edge displacement the results of mesh-free method and finite element method have an equal degree of agreement with the experimental results. Indeed the performance of mesh-free method with 15 nodes in each support is better than meshfree analysis with 4 nodes in each support and even better than the finite element analysis.

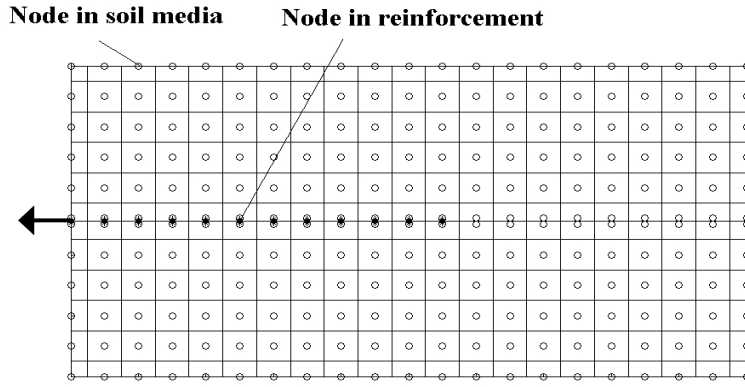


Figure 15. Node arrangement and Voronoi diagram

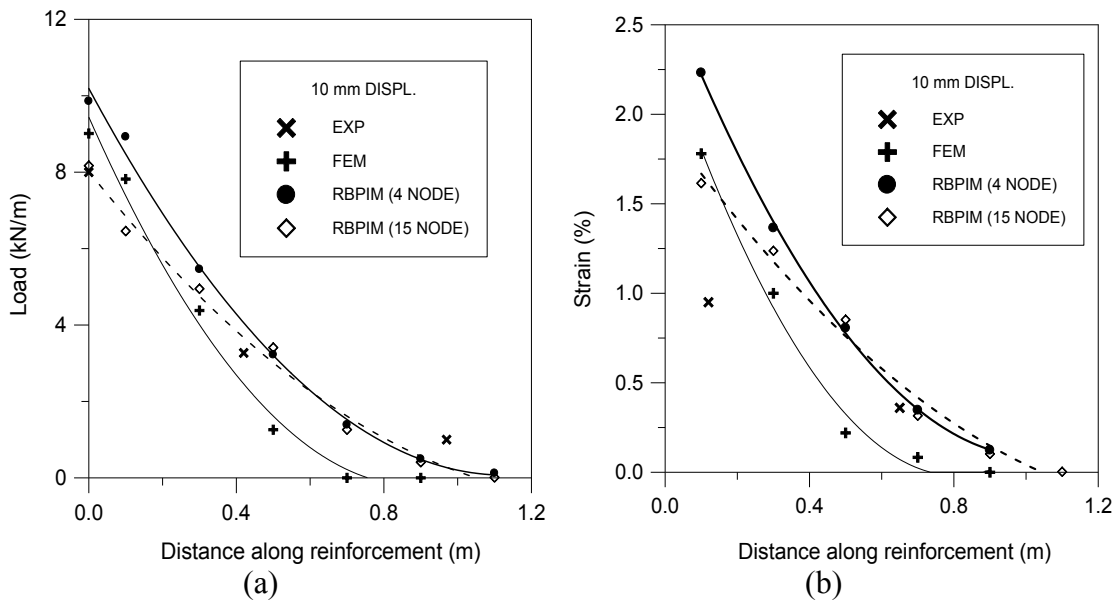


Figure 16. The distribution of (a) load (b) displacement distribution along reinforcement for 10mm edge displacement

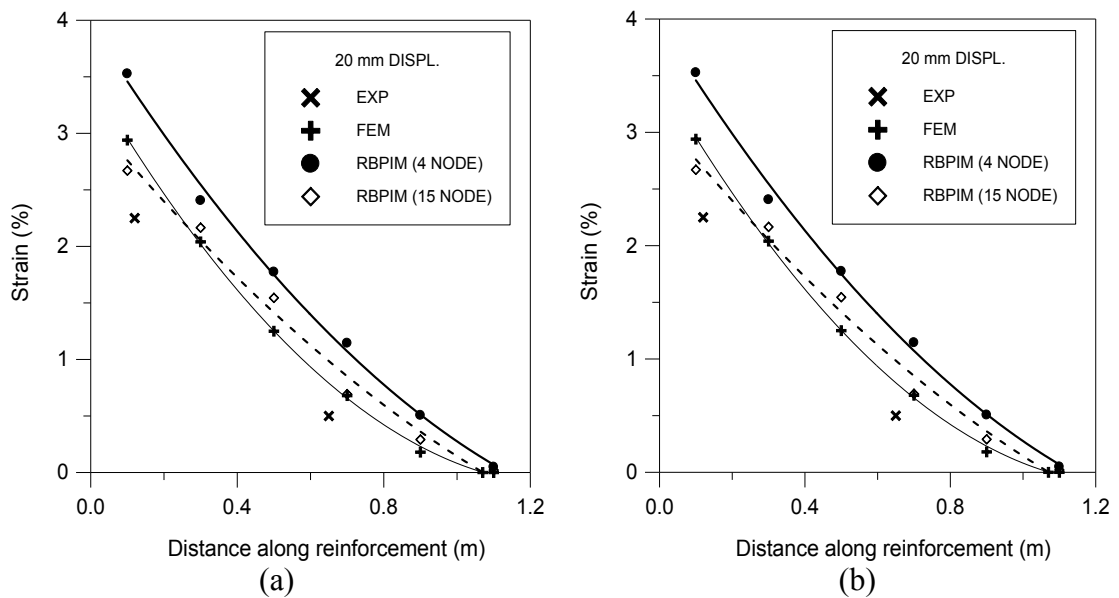


Figure 17. The distribution of (a) load (b) displacement distribution along reinforcement for 20mm edge displacement

6. Conclusions

By the combination of radial basis point interpolation method and the linear conformal nodal integration approach, a truly mesh-free technique is implemented for the elasto-plastic analysis of a discontinuous medium. The discontinuity in the media is simulated by assuming an interface layer between different materials and, the linkage element concept is adopted, to consider the effect of interface layer in the global stiffness matrix. Agreement between the results of proposed mesh-free method and the results of finite element modeling with a high number of elements, or experimental modeling, confirms the robustness and accuracy of proposed method for the elasto-plastic analysis of discontinuous mediums.

References

- [1] A. Zhang, X. Cao, F. Ming, Z. Zhang, Investigation on a damaged ship model sinking into water based on three dimensional SPH model, *Applied Ocean Research*, 42 (2013) 24-31.
- [2] A. Rezaei Mojddehi, A. Darvizeh, A. Basti, Three dimensional static and dynamic analysis of thick plates by the meshless local Petrov-Galerkin (MLPG) method under different loading conditions, *Computational Methods in Civil Engineering*, Vol. 2, 1 (2011) 65-81.
- [3] A. Arjangpay, A. Darvizeh, R. Ansari, Gh. Zarepour, Axial buckling analysis of an isotropic cylindrical shell using meshless local Petrov-Galerkin method, *Computational Methods in Civil Engineering*, Vol. 2, 2 (2011) 219-230.
- [4] T. Belytschko, Y.Y. Lu, L. Gu, Element-free Galerkin methods, *International Journal for Numerical Methods in Engineering*, 37 (1994) 229-256.
- [5] W.K. Liu, S. Jun, Y.F. Zhang, Reproducing kernel particle methods, *International Journal for Numerical Methods in Fluids*, 20 (1995) 1081-1106.
- [6] G.R. Liu, Y.T. Gu, A point interpolation method for two-dimensional solid, *International Journal for Numerical Methods in Engineering*, 50 (2001) 937-951.
- [7] B. Nayroles, G. Touzot, P. Villon, Generalizing the finite element method: diffuse approximation and diffuse elements, *Computational Mechanics*, 10 (1992) 307-318.
- [8] C. Duarte, J.T. Oden, An hp adaptive method using clouds, *Computer Methods in Applied Mechanics and Engineering*, 139 (1996) 237-262.
- [9] J.M. Melenk, I. Babuska, The partition of unity finite element method: Basic theory and applications, *Computer Methods in Applied Mechanics and Engineering*, 139 (1996) 289-314.
- [10] S.N. Atluri, T. Zhu, A new meshless local Petrov-Galerkin (MPLG) approach in computational mechanics, *Computational Mechanics*, 22 (1998) 117-127.
- [11] J.J. Monaghan, An introduction to SPH, *Computer Physics Communications* 48 (1998) 89-96.
- [12] S. Beissel, T. Belytschko, Nodal integration of the element-free Galerkin method, *Computer Methods in Applied Mechanics and Engineering*, 139 (1996) 49-71.
- [13] P.W. Randles, L.D. Libersky, A.G. Petschek, On neighbors, derivatives, and viscosity in particle codes, *The ECCM Conference*, Munich, Germany (Aug. 31- Sept. 3, 1999).
- [14] J. Bonet, S. Kulasegaram, Correction and stabilization of smooth particle hydrodynamics methods with application in metal forming simulation, *International Journal for Numerical Methods in Engineering*, 47 (1999) 1189-1214.
- [15] J.S. Chen, C.T. Wu, S. Yoon, Y. You, A stabilized conforming nodal integration for Galerkin Mesh-free methods, *International Journal for Numerical Methods in Engineering*, 50 (2001) 435-466.
- [16] G.R. Liu, *Meshfree Methods: Moving Beyond the Finite Element Method*, CRC Press Boca, 2003.
- [17] PLAXIS manual, Finite element code for soil and rock analysis, Rotterdam (Netherland) : A.A. Balkema, 1995.
- [18] I. Yogarajah, K.C. Yeo, Finite element modeling of pull-out tests with load and strain measurements, *Geotextile and Geomembranes*, 31 (1994) 43-54.

